The Impact of Global Warming on ENSO Variability in Climate Records

Zhaohua Wu, Edwin K. Schnieder, Zeng-Zhen Hu

Center for Ocean-Land-Atmosphere Studies
4041 Powder Mill Rd., Suite 302
Calverton, MD 20705

and

Liqing Cao

Department of Hydrology and Water Resources
Hehai University
Nanjing 210024
PR. China

ABSTRACT

The variability of ENSO, the largest interannual climate variation of the Pacific ocean-atmosphere system, and its relation to the Pacific Decadal Oscillation and global warming are documented. Analysis using the Empirical Mode Decomposition method, which is useful for analyzing nonlinear, nonstationary climate records, reveals that ENSO contains strong seasonal, biannual, decadal signals, as well as a monotonic trend that is shown to be tied closely to global warming. The frequencies of the interannual components of ENSO are higher when the decadal components of ENSO are in the warm phase, and are also increasing with the global warming trend. It is also argued that the decadal signals and the trend are connected to for the abnormal ENSO events in the 1990s.

1. Introduction

The El Niño and the Southern Oscillation phenomenon (ENSO) is often thought as an irregular interannual oscillator that swings between warm and cold sea surface temperature (SST) and low and high surface pressure over the central and eastern tropical Pacific (Philander 1990). ENSO is the primary driver of interannual climate variability (National Research Council 1996), and has a large economic and social impact over the globe (Glantz et al. 1991). Unusually strong warm events (El Niños) in 1982/83 and 1997/98, along with a long-lasting warm event from 1990 to 1995, raise the question of whether the global warming apparently related to human activities (IPCC 2001) contributes, or will contribute to the tendency for more frequent El Niño events and fewer La Niña (cold) events (Trenberth and Hoar 1996).

Theoretical studies have provided some supporting evidence for variation of the mean state on decadal timescale affecting ENSO variability. Kirtman and Schopf (1998) showed that the mean state change of decadal timescale, rather than the atmospheric noise, is responsible for the change in ENSO frequency and predicability in an intermediate coupled model. In their case, the decadal variation of the mean state does not necessarily require an external cause. However, others have proposed that anthropogenic climate change or interaction between the tropical and midlatitude oceans via thermocline subduction and ventilation could produce mean state change (Gu and Philander 1997). Fedorov and Philander (2000) demonstrated that mean fluctuations of decadal timescale (including the possible trend) do contribute significantly to the later unusual ENSO events, and suggested that global warming cannot be ruled out as a suspect.

In the meanwhile, several linear statistical models have been applied to climate records to address this question (Trenberth and Hoar 1996, Rajagopalan et al. 1997, 1999, Harrison and Larkin 1997, Wunsch 1999), but the answers are not conclusive due to the high sensitivity of model results to model parameters (Rajagopalan et al. 1997, 1999, Harrison and Larkin 1997), especially when stochastic processes are taken into account (Wunsch 1999). In addition to that, linear models implicitly assume that the climate records are stationary and linear, which is highly questionable.

Here, we present results from analyzing climate records using Empirical Mode Decomposition method (EMD) (Huang et al. 1998). The recently developed EMD facilitates the decomposition of climate records in terms of natural oscillatory patterns and trends. Our results suggest that the recent global warming, along with decadal climate variability, contributes not only to the more extreme warm events, but also to more frequent, long lasting ENSO events.

The paper is arranged as the following: section 2 will describe the general properties of the EMD and the climate records that will be analyzed. A brief introduction of the EMD can be found in appendix A. The results using the EMD analysis will be presented in section 3. We will discuss and summarize the results in section 4.

2. Method and Data

The EMD is a recently developed method that can be applied to study the nonlinear and non-stationary properties of a time series (see appendix A for more details). The EMD naturally separates nonlinear oscillatory patterns of higher frequencies from those of lower frequencies and a trend. Through the Hilbert Transform of each purely

oscillatory mode, one can also obtain instantaneous frequency for that mode. In addition to that, the EMD is very efficient: for a time series of length *N*, it usually needs only $log_2 N$ oscillatory modes and a trend to constitute a complete and practically orthogonal set.

We use the EMD to examine the ENSO variability and its relation to the mid-latitude climate variability and global warming. The climate records being examined in this study includes the Southern Oscillation Index (SOI) from January 1866 to December 1997 (Trenberth 1984), the globally averaged surface temperature of the same period (Jones et al. 1999), and the Pacific Decadal Oscillation (PDO) index from January 1900 to December 1999 (Mantua et al. 1997). In all these records, climatological annual cycles have been removed. The SOI is a normalized sea level pressure index that reflects primarily the large-scale dynamics in the tropical Pacific. A large negative (positive) peak of SOI corresponds to a strong El Niño (La Niña) event. The PDO index is the principle component of the leading EOF of the North Pacific SST. Since the Tahiti record used for the calculation of the SOI is less reliable and contains missing data prior to 1935, the focus in this study will be mainly on the climate records after 1935.

3. Results

Some of the IMFs calculated from the SOI are related to physical phenomena, which is evident from Fig. 1. c_1 may be the noise that is contained in the SOI. c_2, c_3, and c_4 correspond to semiannual, annual and biennial cycles, respectively. The semiannual cycle reflects the migration of the sun that crosses the Equator twice a year. The annual cycle of the SOI is still quite strong, which is understandable: the annual cycles that have been

removed from Tahati and Darwin pressures are only the averages and the SOI still contains the remainders of the varying annual cycles. Nonlinear processes are also involved; otherwise, we would not see the strong variation of the amplitude of this mode. The biennial cycle, which was detected by Rasmusson et al. (1990), could result from the nonlinear response of tropical atmosphere to the seasonally varying forcing, or from the interaction between the south Asian monsoon and large-scale circulations in the tropics and extratropics (Meehl 1997, Kim and Lau 2001). The biennial signal is considered an important fact to the boreal spring barrier of the Southern Oscillation persistence (Clarke and Gorder 1999). c_5 and c_6 are interannual modes, with averaged periods of 3.3 and 5.9 year, respectively. These two modes probably represent the oscillators induced by the atmosphere-ocean interaction (Suarez and Schopf 1988, Battisti and Hirst 1989, Jin 1996). The physical cause of decadal modes (c_7, c_8, and c_9) are not at all clear. However, they are possibly related to the atmosphere-ocean interaction of longer time scales or may be the responses of the tropical Pacific to decadal forcings, which will be discussed later.

Most of modes of the SOI are signals. The details of distinguishing signal from noise are discussed in appendix B.

The combination of the interannual components of the SOI only has a moderate amplitude (the upper panel of Fig. 2), and relatively strong ENSO events in the later record are not reflected. However, when the annual mode and the biennial mode are added, the extremely strong events in 1972/73, 1982/83, and 1986/87 are much better defined. Therefore, not only are the interannual modes phase-locked to the seasonal cycle

(Tziperman et al. 1994, Chang et al. 1994), but the annual mode, biennial mode, and their variations also contribute significantly to forming strong ENSO events.

The decadal modes and the trend also contribute significantly to the later ENSO events both in amplitude and duration (the lower panel of Fig. 2). Without the decadal signals and the trends, the prolonged weak El Niño (negative SOI) from later 1990 to later 1995 is much weaker and has much shorter duration, and a much stronger La Niña, and a much weaker El Niño would appear in 1996/97, 1997/98, respectively. Decadal components and the trend contribute almost equally to these abnormalities in the 1990s. If only either the trend or the decadal components is included, the prolonged weak El Niño from later 1990 to 1995 does not appear and the El Niño in 1997/98 is weaker. Therefore, the trend, as well as the decadal variability, is responsible for these abnormal events, which is consistent with Fedorov and Philander (2000).

During the last decade, many modeling efforts have been made to understand the impact of global warming on ENSO variability (Meehl et al. 1993, Tett 1995, Knutson and Manabe 1997, Timmermann 1999). One of the modeling results is the increased El Niño frequency in a climate model forced by future greenhouse warming (Timmermann 1999), a behavior which has not been previously demonstrated through analyzing climate records. The EMD is an ideal tool to examine instantaneous frequency of an oscillatory mode. Our analysis using the new technique appears to agree with the modeling result (Fig. 3): the frequencies of the interannual modes bear a similar pattern and have clear upward trends. In addition to that, the major peaks of frequencies also appear to be located around the peaks of the SOI decadal variability. That relation is less obvious in 1990's when c_5 has very a small amplitude and small errors in Hilbert Transform based

on a time series with limited length could lead to the practical failure to estimate instantaneous frequency accurately.

The related questions are what may be responsible for the ENSO decadal variability and its trend. Our analysis indicates that this may be the response to decadal climate variability in the mid-latitude and global warming (Fig. 4). The multi-decadal mode (c_9) correlates to the decadal components of the PDO index well, with a peak value of 0.98 when the PDO decadal components leads c_9 of the SOI about 2.5 year. This lag relationship could indicate that mid-latitude decadal climate variability forces at least part of the ENSO decadal variability. The SOI trend also has a very large lag correlation with the global warming trend (peaking when the global warming trend leads the SOI trend by 1.5 years), which indicates that global warming is likely to drive more frequent strong El Niño events and less frequent La Niña events in the tropical Pacific.

4. Discussions and Conclusions

In this study, we explored the variability of ENSO (represented by the SOI), and its relation to the Pacific Decadal Oscillation and global warming using a data analyzing method In the EMD that is new to many researchers in climate study community. Our results demonstrated that ENSO not only contains interannual signals, but also contains strong annual, biennial, decadal signals, and a monotonic trend. We also showed that the ENSO multi-decadal component may be, at least partly, driven by decadal variability that happens in the Northern Pacific. The ENSO trend is shown to be tied closely to global warming, with the latter likely driving the former. The frequencies of the interannual

components of ENSO appear to be higher when the decadal components of ENSO are in the warm phase, and are increasing with the global warming trend.

Acknowledgments. The first author is grateful to Dr. E. Sarachik of University of Washington for his helpful suggestions and encouragement. This study was sponsored by NSF under grant ATM 99-07915.

Appendix A

The Empirical Mode Decomposition[1]

For the last two hundred years, many data analysis methods of time-varying series have been developed based on Fourier analysis techniques by breaking down the data into series of linear sinusoidal functions with different amplitude coefficients. In general, these methods can hardly offer information of the variations in amplitude and frequency on the time axis as it adopts the sine and cosine as the basis for the expansion. The empirical mode decomposition (EMD), however, naturally separates the signals of varying amplitude and frequency based on the natural appearance of extremes of a time series without using any pre-defined basis. The detail of the method and examples of application to seismic data, satellite data, and problems of nonlinear mechanics can be found in Huang et al. (1998).

The physical foundation of the EMD is illustrated in Fig. A1. Suppose that there is a receiver to record the overall signal amplitude of the oscillatory signals of varying frequency and amplitude from many transmitters that produce signals in different frequency bands. If the amplitude of the high frequency signal is not extremely small, one would observe that the peaks of the high frequency signal are superimposed on the signals of relatively lower frequency in the record. Based on the information of the extremes, one can extract the signals of higher frequency by recovering the nonlinear

[1] The EMD and the corresponding Hilbert-Huang Transform received the Research and Development (R&D) 100 Awards of 2002 for its groundbreaking success in analyzing nonlinear and non-stationary data. A commercial software for performing the EMD analysis and Hilbert-Huang Transform is available from Princeton Satellite Systems Inc., Princeton, N.J.

oscillatory pattern with varying frequency and amplitude. The detailed process called "sifting through envelopes" will be discussed later.

Such a physical idea is useful for analyzing climate records. The complicated climate records usually contain noise and errors, signals of synoptic weather perturbations, seasonal variations, and other variations either being driven by varying external forcing or due to internal nonlinear dynamics of the system. In general, the frequency bands of variations of different time scale are well separated. Therefore, the EMD method is conceptually useful to extract important information hidden in the climate records.

Mathematically, for a climatic time series $f(t)$, the EMD separates the series into a limited number of modes, i.e.,

$$f(t) = \sum_k c_k(t) + r, \tag{A1}$$

where $c_k(t)$ is a pure oscillatory pattern called the Intrinsic Mode Function (IMF) with zero mean [see Huang et al. (1998) for a more rigorous definition], and r is usually monotonic and called the trend. In practice, the EMD is very efficient: for a time series of length N, it usually only needs $log_2 N$ IMFs and a trend to constitute a set that is complete and practically orthogonal in Lie sense.

a. Sifting through envelopes

The actual separation method is called "sifting through envelopes". Suppose one has a time series such as the bold line in panel *a* of Fig. A2. One first finds the local maximums and minimums of that time series, and then connects the local maximums and local

minimums with two smooth lines[2]. These two lines define the upper envelope and the lower envelope. The mean of these two envelopes are shown by the thin solid line in panel *a* of Fig. A2. This mean is defined as the reference line for the time series. By subtracting the mean from the original time series, one obtains a much better defined oscillatory pattern h_1 (the solid line in panel *b* of the Fig. A2).

However, h_1 is still not a pure oscillatory pattern with upper envelope and lower envelope being symmetric about the $y = 0$ axis. By repeating the sifting process, the oscillatory pattern eventually converges to an IMF (the bold line) as shown in panel *c* of Fig. 2A.

Clearly, the final IMF contains many more oscillatory peaks than those are seen in the original time series. However, these peaks are not artificially generated, which is evident from the observation of the reminder (the original time series subtracting the IMF). In panel *d* of Fig. 2A, the reminder (the thin solid line) is overlapped on the original time series. Clearly, the remainder is a natural smooth fitting to the original time series, but still containing variabilities of lower frequencies.

Identical processes of sifting are applied to the reminder to obtain more IMFs of lower frequencies until a monotonic trend is obtained.

b. Instantaneous frequency

The instantaneous frequency can be obtained through the Hilbert Transform. For a purely oscillatory mode $c_k(t)$, its Hilbert transform is defined as

[2] In this study, the cubic spline interpolation is used to obtain the smooth lines in the first derivative and continuous in the second derivative, both within an interval and at its boundaries. The details of this method can be found in Press et al. (1992).

$$b_k(t) = \frac{1}{\pi}\int_{-\infty}^{\infty}\frac{c_k(t')}{t-t'}dt' . \quad \text{(A2)}$$

$c_k(t)$ and $b_k(t)$ can be combined into a complex expression as

$$z_k(t) = A_k(t)exp\left[i\phi_k(t)\right], \quad \text{(A3)}$$

where $A_k(t) = \sqrt{c_k^2(t) + b_k^2(t)}$ is the envelope of the nonlinear oscillatory pattern $z_k(t)$, and $\phi_k(t) = arctan\left[b_k(t)/c_k(t)\right]$, defining the phase angle. From Eq. (A3), one can obtain the instantaneous frequency through the calculation of the derivative of $\phi_k(t) = arctan\left[b_k(t)/c_k(t)\right]$ with respect to t, i.e.,

$$\omega_k(t) = d\phi_k(t)/dt . \quad \text{(A4)}$$

In practice, there are several popular methods to practically estimate the Hilbert Transform (Barnett 1983). In this study, convolution method of Oppenheimer and Schäfer (1975) is used.

The calculation of instantaneous frequency produces meaningful results when it is applied to the pure oscillatory IMFs but can be misleading when applied to the original full time series. We will report this issue along with our improvement of the EMD and its capability of dealing with noise in near future.

Appendix B

Signal and Noise of IMFs

A related important issue is whether most IMFs are "signals" or "noises". Decomposition of a white noise series of the same length as that of the SOI obtains the same numbers of modes that have varying amplitudes and frequencies along the time axis. To distinguish the signals from noises, we examine the energy of all IMFs, which is defined as the integration of the square of the amplitude of the IMF over the whole time domain, of both white noise and the SOI. Theoretically, we can infer that a hyperbola fits the energies of the IMFs of white noise. (Details of derivation will be reported elsewhere.) The upper panel of Fig. B1 gives an example of the energy distribution of each IMF of a white noise series and the hyperbolic fitting.

Based on the energy property of the IMFs of white noise, we can introduce a criterion to distinguish signals from noise for the SOI. If the SOI contains white noise, each IMF of the SOI contains a component of white noise. The energy of noise component fits a hyperbola. Assuming that c_1 of SOI is all from white noise and contains no signal, then the energy level of c_1 can be used as the reference point for the white noise in the SOI. A hyperbola passing through energy level of c_1 can then serve as the base line of signals, and any IMF whose energy level is far above that base line can be regarded as signal. Clearly, the base line is an overestimation of noise if c_1 contains any signal.

The distribution of the energy of each mode of SOI is illustrated in the lower panel of Fig. B1. Clearly, the energies of IMFs three to nine are all well above the base line and therefore these modes are most signals.

References

Barnett, T. P., 1983: Interaction of the monsoon and Pacific trade wind system at interannual time scale. Part I: the equatorial zone. *Mon. Wea. Rev.*, **111**, 756-773.

Battisti, D. S., and A. C. Hirst, 1989: Interannual variability in a tropical atmosphere-ocean model: Influence of the basic state, ocean geometry and nonlinearity. *J. Atmos. Sci.*, **46**, 1687-1712.

Chang, P., B. Wang, T. Li, and L. Ji, 1994: Interactions between the seasonal cycle and ENSO—frequency, entrainment, and chaos in a coupled atmosphere-ocean model. *Geophys. Rev. Lett.*, **21**, 2817-2820.

Clarke, A. J., and S. V. Gorder, 1999: On the connection between the boreal spring southern oscillation persistence barrier and the tropospheric biennial oscillation. *J. Climate*, **12**, 610-620.

Fedorov, A. V., and S. G. Philander, 2000: Is El Niño Changing? *Science*, **288**, 1997-2002.

Glantz, M. H., R. W., Katz, and N. Nicholls (eds.), 1991: *Teleconnections Linking Worldwide Climate Anomalies*, Cambridge University Press, 535pp.

Gu, D., and S. G. Philander, 1997: Interdecadal climate fluctuation that depend on exchanges between the Tropics and the extratropics. *Science*, **275**, 805-807.

Harrison, D. E., and N. K. Larkin, 1997: Darwin sea level pressure, 1876-1996: evidence for climate change? *Geophys. Rev. Lett.*, **24**, 1779-1782.

Huang, N. E., Z. Shen, S. R. Long, M. C. Wu, H. H. Shih, Q. Zheng, N.-C. Yen. C. C. Tung, and H. H. Liu, 1998: The empirical mode decomposition and the Hilbert spectrum for nonlinear and non-stationary time series analysis. *Proc. R. Soc. Lond.*, **454A**, 903-995.

IPCC, 2001: *Climate change 2001: The Scientific Basis. Contribution of Working Group I to the Third Assessment Report of the Intergovernmental Panel on Climate Change*, Cambridge University Press, 881pp.

Jin, F.-F., 1996: Tropical ocean-atmosphere interaction, the Pacific cold tongue, and the El Niño-Southern Oscillation. *Science*, **274**, 76-78.

Jones, P. D., M. New, D. E. Parker, S. Martin, and I. G. Rigor, 1999: Surface air temperature and its changes over the past 150 years. *Rev. Geophys.*, **37**, 173-199.

Kim, K.-M., and K.-M. Lau, 2001: Dynamics of monsoon-induced biennial variability in ENSO. *Geophys. Rev. Lett.*, **28**, 315-318.

Kirtman, B. P., and Schopf, 1998: Decadal variability in ENSO predictability and prediction. *J. Climate*, **11**, 2804-2822.

Knutson, T. R., S. Manabe, and D. Gu, 1997: Simulated ENSO in a Global Coupled Ocean–Atmosphere Model: Multidecadal Amplitude Modulation and CO_2 Sensitivity. *J. Climate,* **10**, 138-161.

Mantua, N. J., S. R. Hare, Y. Zhang, J. M. Wallace, and R. C. Francis, 1997: A Pacific interdecadal climate oscillation with impacts on salmon production. *Bull. Amer. Meteor. Soc.*, **78**, 1069-1079.

Meehl, G. A., 1997: The south Asian Monsoon and the tropospheric biennial oscillation. *J. Climate*, **10**, 1921-1943.

Meehl, G. A., G. W. Brantstator, and W. M. Washington, 1993: Tropical Pacific interannual variability and CO_2 climate change. *J. Climate,* **6**, 42-63.

National Research Council, 1996: *Learning to Predict Climate Variations Associated with El Niño and the Southern Oscillation*, National Academy Press, 171pp.

Oppenheimer, A. V., and R. W. Schäfer, 1975: *Digital Signal Processing*. Prentice Hall, 360pp.

Press, W. H., S. A. Teukolsky, W. T. Vetterling, and B. P. Flannery, 1992: *Numerical recipes in FORTRAN: the art of scientific computing.* Cambridge University Press, 963pp.

Philander, S. G., 1990: *El Niño, La Niña, and the Southern Oscillations*, Academic Press, 293pp.

Rajagopalan, B., U. Lall, and M. A. Cane, 1997: Anomalous ENSO occurrences: an alternate view. *J. Climate*, **10**, 2351-2357.

Rajagopalan, B., U. Lall, and M. A. Cane, 1999: Comment on "Reply to the Comments of Trenberth and Hurrell". *Bull. Amer. Meteor. Soc.,* **80**, 2724-2726.

Rasmusson, E. M., X. Wang, and C. F. Ropelewski, 1990: The biennial component of ENSO variability. *J. Mar. Syst.*, **1**, 71-90.

Suarez, M. J., and P. S. Schopf, 1988: A delayed action oscillator for ENSO. *J. Atmos. Sci.,* **45**, 3283-3287.

Tett, S., 1995: Simulation of El Niño-Southern Oscillation-like variability in a global AOGCM and its response to CO_2 increase. *J. Climate,* **8**, 1473-1502.

Timmermann, A., J. Oberhuber, A. Bacher, M. Esch, M. Latif, and E. Roeckner, 1999: Increased El Niño frequency in a climate model forced by future greenhouse warming. *Nature*, **398**, 694-687.

Trenberth, K. E., 1984: Signal versus noise in the Southern Oscillation. *Mon. Weather Rev.*, **112**, 326-332.

Trenberth, K. E., and T. J. Hoar, 1996: The 1990-1995 El Niño-Southern Oscillation event: Longest on record. *Geophys. Rev. Lett.*, **23**, 57-60.

Tziperman, E., L. Stone, M. Cane, and H. Jarosh, 1994: El Niño chaos: overlapping of resonances between the seasonal cycle and the Pacific ocean-atmosphere oscillator. *Scinece*, **264**, 72-74.

Wunsch, C., 1999: The interpretation of short climate records, with comments on the North Atlantic and Southern Oscillations. *Bull. Amer. Meteor. Soc.*, **80**, 245-255.

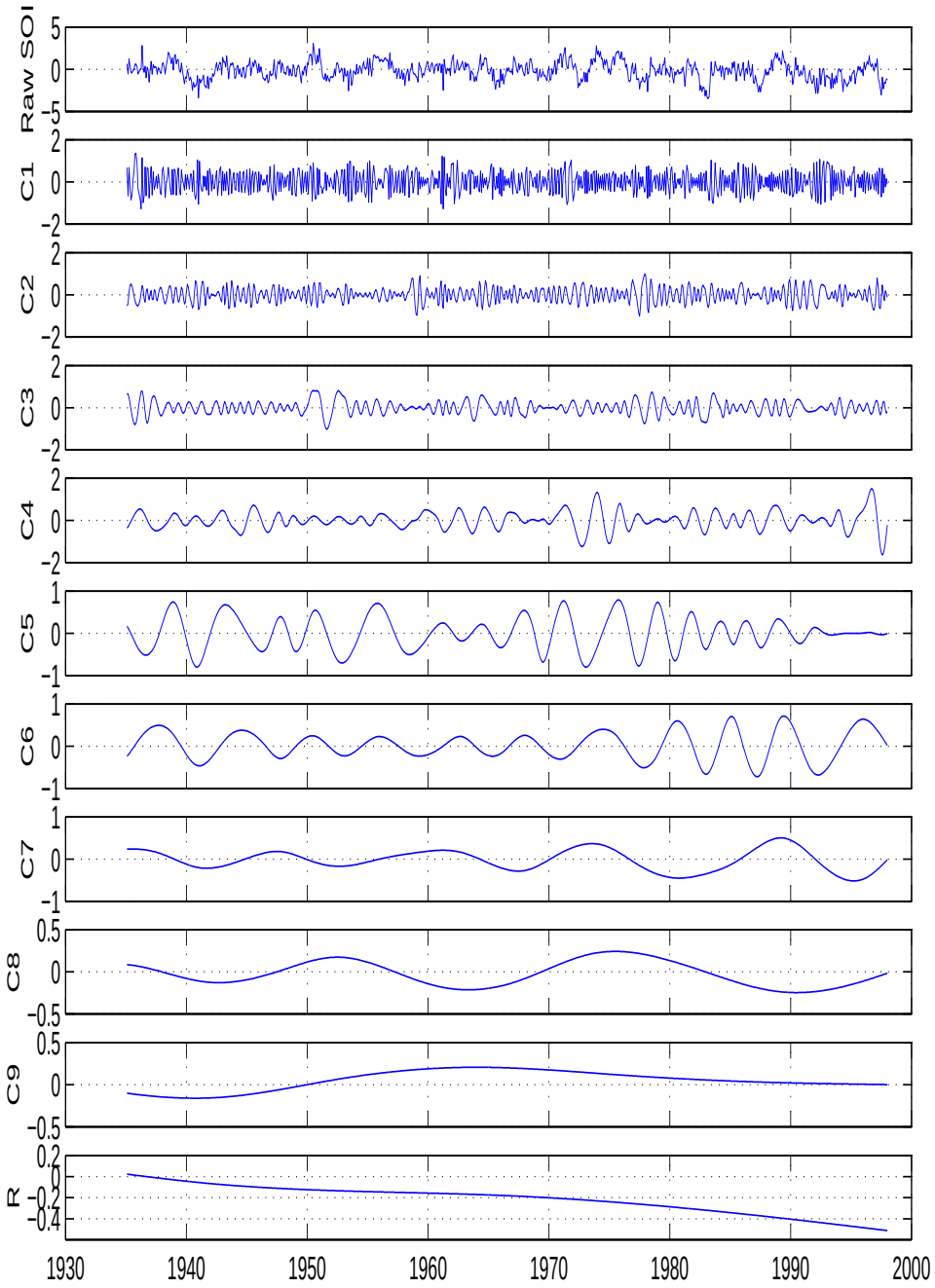

Fig. 1: The raw SOI index (top panel), the corresponding intrinsic mode functions (C1-9), and the monotonous trend.

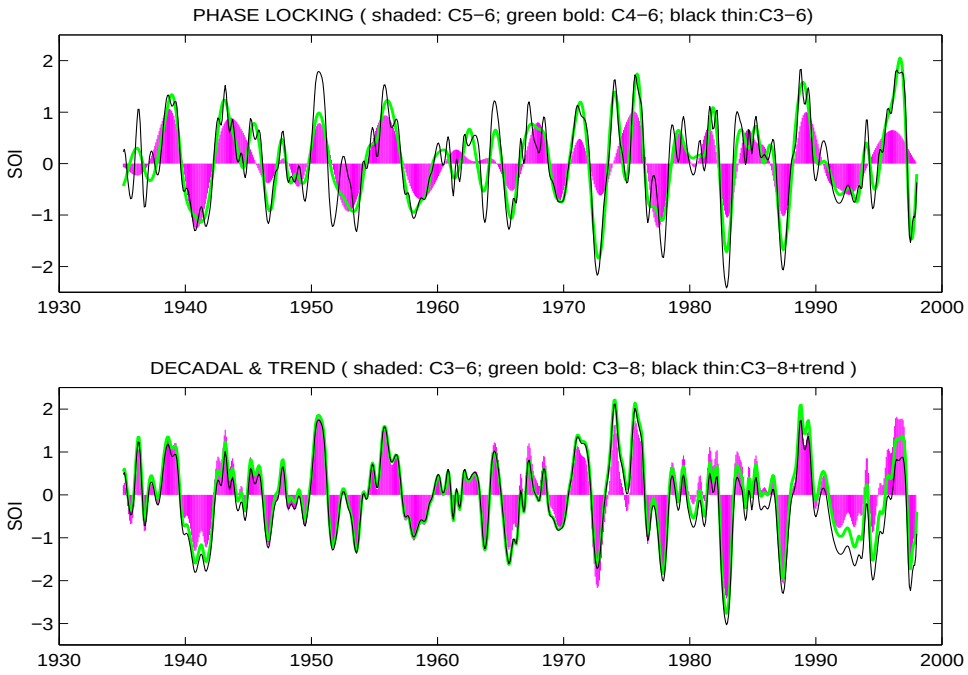

Fig. 2: The high frequency components of SOI (upper panel): the interannual components (*C5,6*, shaded); the interannual plus the biennial components (*C4-6*, green bold line); and the sum of the annual, the biennial, and interannual components (*C3-6*, black thin line). The decadal variability and the trend of SOI (lower panel): the high frequency components of SOI (*C3-6*, shaded); the high plus low frequency components of SOI (*C3-9*, green bold line); and the sum of the high, low frequency components, and the trend (*C3-9* and *R*, thin black line).

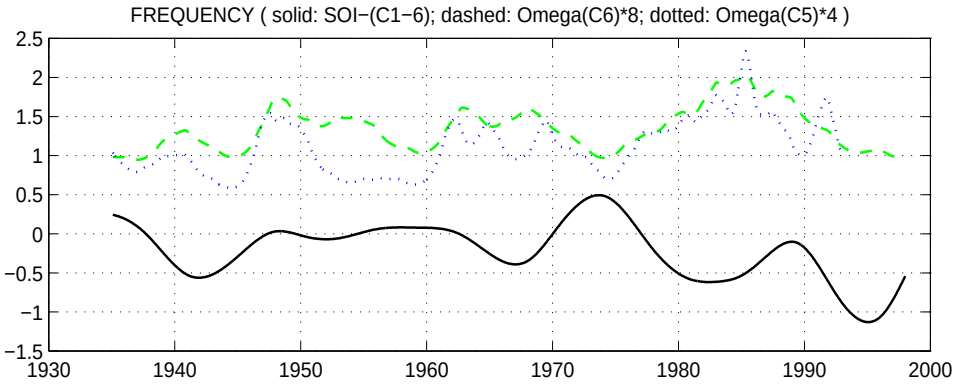

Fig. 3: The long-term variability of SOI and the frequency variation of interannual components of SOI. The black solid line is the sum of the low frequency components and the trend of SOI. The green dashed line is the unsmoothed frequency (phase speed) of *C6* multiplied by a factor 8; and the blue dotted line is the unsmoothed frequency (phase speed) of *C5* multiplied by a factor 4. The SOI components are not scaled. The unit value for the frequency corresponds to one-year period.

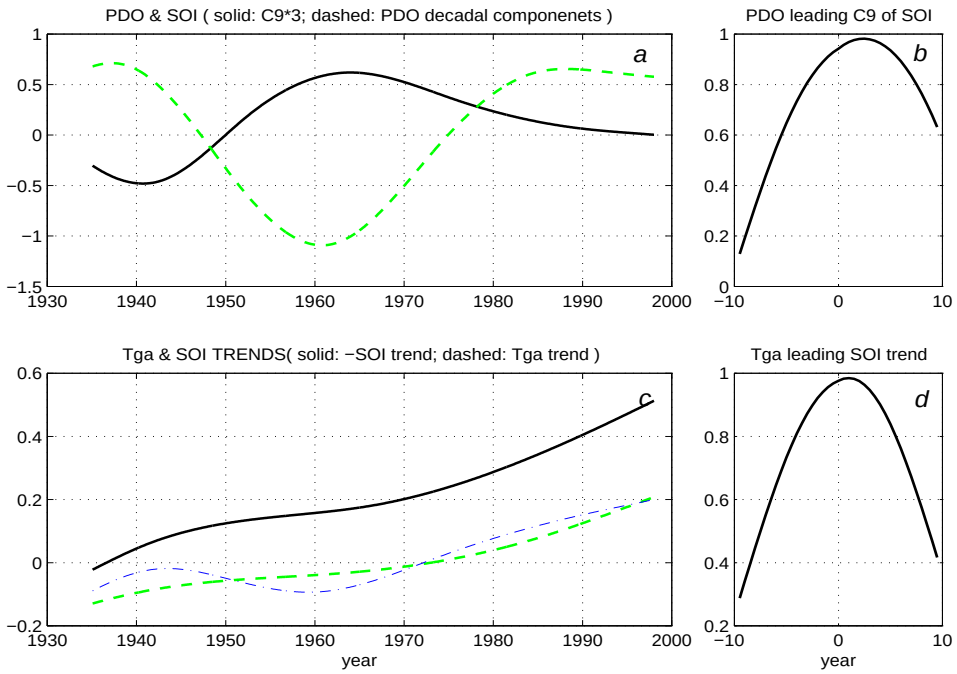

Fig. 4. ENSO, mid-latitude climate variability, and global warming. The upper panel: the multi-decadal component of SOI multiplied by a factor of 3 (solid line), and the decadal components of the Pacific Decadal Oscillation (PDO) index. The lower panel: the trend of SOI multiplied by (-1) (black solid line), the trend of the globally averaged temperature anomaly (with a unit Kelvin, green dashed line). The blue dash-dotted line is the sum of the multi-decadal component and the trend of the globally averaged temperature anomaly, which can be viewed as a smoothed version of the globally averaged temperature anomaly seen in many scientific papers and documents.

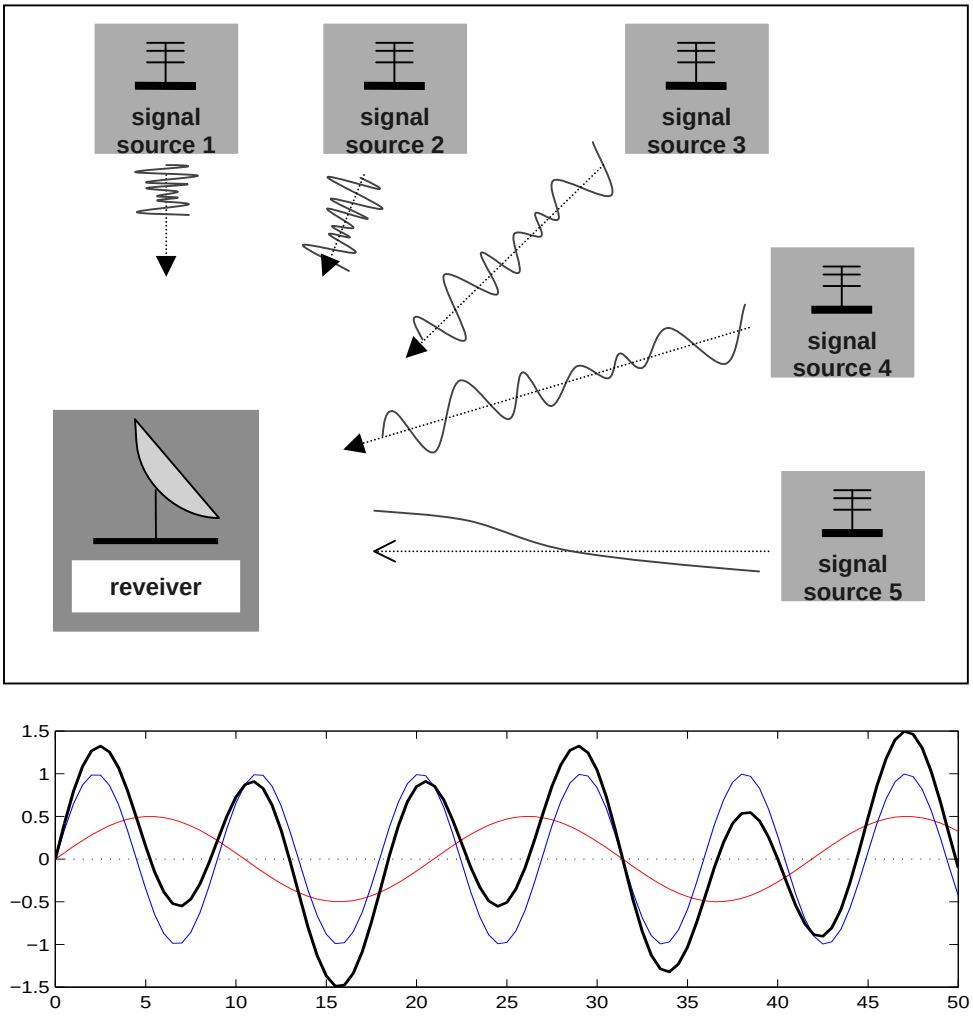

Fig. A1. Upper panel: the schema for the physical meaning of the EMD. The different signal sources send out the pure oscillatory signals of different frequency bands. A receiver records the overall signal amplitude. Lower panel: the red and blue thin lines represent the pure oscillatory signals from two sources; and the bold line represents the overall signal recorded by the receiver. The EMD can separate accurately the two unique oscillatory patterns based on the recorded overall signal.

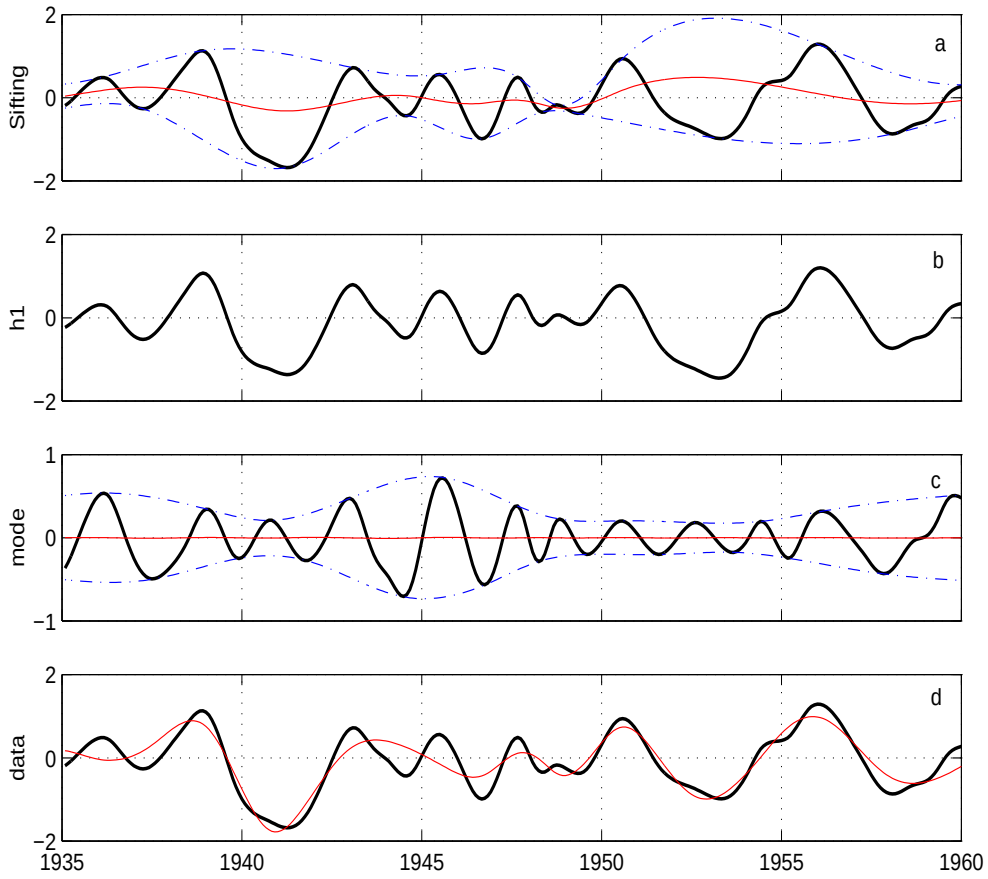

Fig. A2. The sifting process. Panel *a*: the bold solid line is the original time series; the dash-dotted lines represent the upper and the lower envelopes, respectively; and the thin solid line is the mean of the envelopes. Panel *b*: the solid line represents the difference between the original data and the mean defined in panel *a*. Panel c: the bold solid line is an IMF obtained from the sifting process. Panel *d*: the bold solid line is the original time series; and the thin line represents the difference of the original data and the IMF obtained.

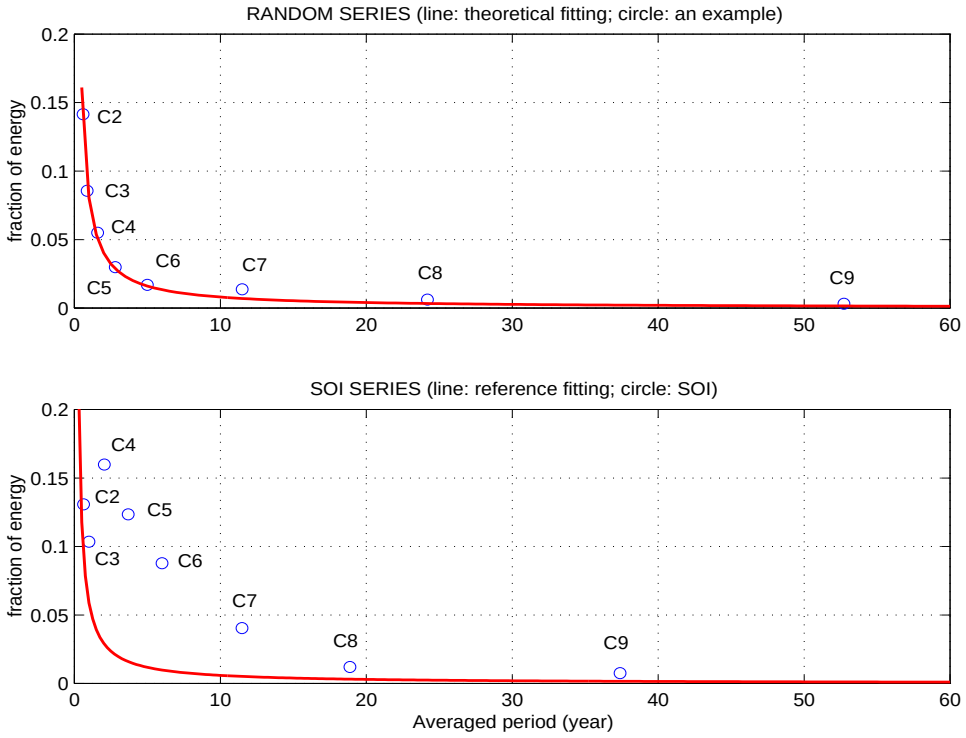

Fig. B1: The energy of IMFs of white noise (upper panel) and the SOI (lower panel). The circles of both panels mark the energy levels of each mode along the axis of the averaged period of that mode. The red line is the theoretical fitting line for white noise contained in a time series.